Effect of the temperature of cerium nitrate–NaCl solution on corrosion inhibition of mild steel

Hichem Boudellioua, Youcef Hamlaoui, Lakhdar Tifouti, Fernando Pedraza

HAL Id: hal-02466332
https://hal.science/hal-02466332

Submitted on 4 Feb 2020

Effect of Temperature of Cerium Nitrate-NaCl Solution on Corrosion Inhibition of Mild Steel

H. Boudellioua[1]*, Y. Hamlaoui[2], L. Tifouti[1], F.Pedraza[3]

1. Laboratoire de Génie de l'Environnement (LGE), Université Badji Mokhtar, BP 1223, 23020 El Hadjar-Annaba, Algérie.

2. Laboratoire de Physique de la Matière et Rayonnement (LPMR), Faculté des Sciences et de Technologie, Université Mohamed Chérif Messaadia, BP 1553, 41000 Souk-Ahras, Algérie.

3. Laboratoire des Sciences de l'Ingénieur pour l'Environnement (LaSIE, UMR-CNRS 7356), Université de La Rochelle, Avenue Michel Crépeau, 17042 La Rochelle Cedex 1, France.

Abstract

In this work, the effect of temperature on corrosion inhibition was studied in the absence and presence an optimal concentration of cerium nitrate (600 mg.L^{-1}) as an inhibitor of mild steel in sodium chloride. Corrosion tests were carried out through electrochemical techniques such as impedance spectroscopy and d.c polarization measurements. The surface morphology of the films was investigated by optical microscopy (MO), white light interferometry (WLI) and a scanning electronic microscopy (SEM) coupled to EDS analysis for chemical composition. The results obtained show that the activation energy for the corrosion inhibition process to occur increased in the presence of cerium nitrate inhibitor. However, the corrosion resistance of mild steel was somewhat lost with increasing the solution temperature up to 55 °C, which lead to more cracked films. The enthalpy and entropy values suggested a mixed mechanism of chemisorption and physisorption inihibition, with a major dominant of physisorption control.

Keywords: Cerium nitrate; Inhibition; Temperature; Enthalpy; Physisorption; Surface morphology.

1. Introduction

Temperature may modify the interaction mechanisms between the metal and aggressive media in the presence of inhibitors, because many changes occur on the metal surface such as rapid etching and desorption of inhibitor molecules while the inhibitor itself may decompose [1].

The inhibition efficiencies impaired by cerium as an inhibitor are commonly dependent on different factors including oxygen reduction (to increase local pH), the extent of corrosion before the formation of the Ce hydroxide film, and the solubility products of hydroxide to reach precipitation. All these factors depend on temperature. Furthermore, the changes in temperature contribute to increase the particle size of the deposits [2]. Upon the elaboration of cathodic electrodeposits of cerium oxy-hydroxides, the microstructure and the morphology of the barrier films were also significantly modified by the temperature of the electrolytic bath [3-4]. Arurault *et al.* noted that when the temperature was increased, a change in the interfacial pH occurred thereby modifying the crystallite size and the morphology of the ceria-based films [5]. Zhou *et al.* found that the grain size of the film deposited on 430 stainless steel increased from 6 to 16 nm with increasing the bath temperature from 26 to 80°C, which made the film less compact [6]. The same remarks were made by Wang *et al.*[7]. In addition to the increase in crystallite size, Hamlaoui *et al.* reported that number of oxygen vacancies of the electrodeposited ceria-based coatings also increased with temperature and concluded that the presence of such defects was not adequate for corrosion protection [3]. Similarly, Zhou *et al.*[6] also reported that the shape of crystallites was modified by the temperature of the solution. For instance, the square-like grains at 30°C became hexagonal at higher temperatures. These changes in shape are related to a modification in growth rate of the planes (100) and (111) of the fluorite cubic structure. However, there are no thorough studies on mild steel when exposed to NaCl media containing cerium nitrate as corrosion inhibitor instead of cathodic electrodeposits made from, which is the purpose of this work. The main objective of the present work is to understand the

inhibition mechanism of corrosion exerted by cerium nitrate inhibitor on the mild steel surface. Here, the effects of the temperature on the inhibition ability of cerium nitrate on steel immersed for 30 min in 0.1M NaCl medium were studied between 25 and 55°C (298-328K) to avoid excessive evaporation of the solution by using potentiodynamic polarization and EIS techniques.

2. Experimental

2.1. Materials and solution preparation

The samples (ASTM A915 mild steel) were cut from a bar with a diameter of 1 cm. A copper wire was welded to the back side and the whole embedded in epoxy resin leaving an exposed area of 0.95 cm^2 (i.e. the edges of the samples were not exposed). Thereafter, the samples were abraded with emery paper from SiC#320 to SiC#4000, washed with distilled water, degreased with ethanol, rinsed again with distilled water to remove ethanol traces, and finally dried with cool-air stream. This preparation step was carried out immediately before immersion of the samples in the solutions to perform the corrosion tests.

The corrosion tests were carried out in 0.1M NaCl solutions at different temperatures 25, 35, 45 and 55°C. The solutions were gently stirred to obtain a slight vortex of the electrolyte to aerate naturally the solutions.

The inhibitor was directly dissolved in the corrosive medium. The concentration of cerium nitrate, $Ce(NO_3)_3,6H_2O$ (Sigma-Aldrich, Mw = 434.22; 99.9%) used in this study was 600 mg.L^{-1}, which was found to be optimal for providing corrosion protection in sodium chloride [8].

In the absence of cerium nitrate inhibitor (only with 0.1M NaCl), the pH and conductivity (λ) of the solution are 6.5 and 9.8 µS.cm^{-1}, respectively. The addition of cerium nitrate inhibitor decrease the pH to 5.2; and increase the conductivity of the solution to 12.2 µS.cm^{-1}.

2.2. Electrochemical measurements

The electrochemical experimental set-up was composed of a classic three electrodes cell using a platinum wire as counter electrode (CE) surmounted with a saturated calomel electrode (SCE, 0.24 V vs. NHS) as the reference one, and mild steel sample as working electrode (WE).

The electrochemical measurements were performed using a PGZ 301 (Voltalab 40 model) potentiostat/galvanostat coupled to a frequency response analyzer (FRA) Volta Master IV software. The working electrodes were immersed in the aerated 0.1M NaCl solution with and without additions of cerium nitrate at different temperatures of the bath. The potentiodynamic polarization curves were obtained by using a sweep rate of 0.5 mV.s^{-1} between ±250 mV compared to the corrosion potential (E_{corr}). The resistance polarization values (R_p) were carried out between ±20 mV around the corrosion potential (E_{corr}), and at 0.167 mV.s^{-1} of scan rate. The impedance data were obtained at the corrosion potential (E_{corr}) between 100 KHz and 5 mHz, with 4 mV as the applied sinusoidal perturbation. The EIS response from the samples was fitted using ZView software. The potentiodynamic polarization and EIS techniques were recorded after 30 minutes of immersion time.

All the corrosion tests were repeated at least from two to three times for reproducibility purposes.

2.3. Morphology of the films

Non-contact white-light optical profilometry was performed using a WLI FL FRT. Imaging of the surface of the samples was conducted using vertical scanning interferometry (VSI) mode with full resolution. Analysis of the surface roughness, thickness and grain size was calculated using FRT Mark III software. Surface analysis was also performed using Zeiss Axio Imager M1 Trinocular Frame optical microscope. Moreover, the surface morphology was analysed

more thoroughly by scanning electron microscope (SEM) of FEI QUANTA 250 equipped with an X-ray energy dispersive spectroscopy (EDS) for chemical analysis of films.

3. Results and discussion

The potentiodynamic measurements and EIS (Nyquist and Bode) techniques are presented in **Fig. 1**. The data extracted from these plots are presented in **Tables 1**.

The use of cerium nitrate as inhibitor to protect the metal against corrosion allowed the formation a film rich in cerium oxy-hydroxides that hindered the diffusion of oxygen, thereby retarding the cathodic reaction at room temperature **[9-11]**. The reaction mechanisms for this to occur are well-known in the current literature **[12-14]**. The polarization resistance (Rp) calculated from the slope (dE/dI) by Ohm's law, and corrosion current density (I_{corr}) can be calculated by using the Stern-Geary polarization resistance method **[15]**, where βa is the anodic Tafel slope (mV/decade).

It is known that the oxygen reduction reaction (1) is the dominant local cathodic process during the corrosion of iron:

$$O_2 + 2H_2O + 4e^- \rightarrow 4OH^-$$ (1)

The anodic reaction is an oxidation process leading to the dissolution of iron can undergo through two different transformations according to reactions (2) and/or (3):

$$Fe \rightarrow Fe^{2+} + 2e^-$$ (2)

$$Fe^{2+} \rightarrow Fe^{3+} + e^-$$ (3)
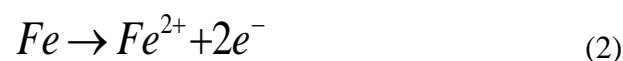
In the non-inhibitedmild steel and irrespective of the temperature (**Fig. 1a**), the slopes of the cathodic domain run almost parallel indicating that the reduction of oxygen to the metal surface

occurred with the same activation mechanism. In contrast, the anodic slopes increased with increasing temperature due to the enhanced metal dissolution. Also, the E_{corr} was shifted to the less noble potentials by raising the temperature. **Table 1** presents the results obtained in **Fig. 1a**, where it was noticed the increase of the current densities with temperature. Commonly, the corrosion product layer become more defective with temperature, a greater attack of chloride ions, of water or of oxygen (or any combination thereof) would be thus expected, hence increasing corrosion.

In the presence of cerium nitrate (**Fig. 1b**), the results are quite different. An increase of both the anodic and cathodic current densities with temperature was observed. This observation suggests that the anodic and cathodic reactions are activated. Also, the corrosion potentials are more negative than in the absence of cerium nitrate. Therefore, the layer formed in the inhibited and in the non-inhibited (bare) NaCl solution should be different. This hypothesis is supported by the corrosion rate (I_{corr}), and polarization resistance (R_p) values, which are drastically reduced in the presence of the inhibitor (Table 1). Also, the I_{corr} and R_p respectively increased and decreased with temperature for both the inhibited and the non inhibited samples. It thus appears that either the film is more defective or that the inhibitor desorbs when the temperature of the solution is raised.

The value of surface coverage (θ) was calculated from the following equation <1>[16]:

$$\theta = \frac{I_{corr} - I_{corr(inh)}}{I_{corr}}\ldots\ldots\ldots<1>$$

where, I_{corr} and $I_{corr(inh)}$ are the corrosion currents densities of mild steel in the absence and presence of cerium nitrate inhibitor, respectively. The surface coverage (θ) values are also gathered in **Table 1**. The surface coverage (θ) did not change when the temperature was risen to 35°C but started to decrease slowly with increasing temperature till 55°C.

The activation energy of the corrosion process to occur in the presence of inhibitor can be derived from the Arrhenius relationship and the current density values from **Table 1** following equation <2>[17].

$$Ln(Icorr) = Ln\,A - \frac{Ea}{RT} \ldots\ldots <2>$$

Where; E_a, R, A, and T are the apparent activation corrosion energy, the gaz constant, the Arrhenius pre-exponential constant and the absolute temperature, respectively.

From the Arrhenius plots shown in **Fig. 2**, the values of E_a with and without cerium nitrate inhibitor on mild steel in NaCl solution were obtained and are summarised in **Table 2**.

An alternative form of the Arrhenius equation allows the determination of the enthalpy and entropy <3>[18].

$$Icorr = \frac{RT}{Nh} exp\left(\frac{\Delta Sa}{R}\right) exp\left(-\frac{\Delta Ha}{RT}\right) \ldots\ldots <3>$$

Where; h (h = 6.63 10^{-34} J.s), N (N = 6.023 10^{23} mole^{-1}), ΔS_a and ΔH_a, are the Planck's constant, Avogadro's number and the entropy and enthalpy of activation, respectively. **Fig. 3** shows the plot $Ln(I_{corr}T^{-1})$ versus $10^3 T^{-1}$. The linear dependency between ΔH_a and the inverse of temperature allowed to calculate ΔH_a from the slope ($\Delta H_a/R$) and ΔS_a from the intercept (ln(R/Nh) + ($\Delta S_a/R$)) (see **Table 2**).

The value of ΔH_a provides information about the mechanism of corrosion inhibition which takes place at the electrochemical interface. The negative sign of ΔH_a shows that the adsorption of inhibitor is controlled by an exothermic process, while the positive sign means the endothermic one. Pournazari *et al.* reported that in an exothermic process, values of $\Delta H_a \geq$ -40 kJ/mol are related to physisorption (less negative values), while $\Delta H_a \leq$ -100 kJ/mol corresponds to chemisorption (more negative values), the values in between being under a mixed control [19]. In our case, the value of about -41 kJ/mol of ΔH_a indicates that the inhibitor is majorly

physically adsorbed on the surface of mild steel. In addition, the negative value of ΔS_a suggests that the activated complex represents an association rather than dissociation between the adsorbed particles of the inhibitor and the corrosion products.

Clearly, the activation energy of the corrosion process is much higher in the presence of inhibitor than in its absence (**Table 2**). This suggests that the film of cerium oxy-hydroxide formed on the surface of steel blocks physically the access of the corrosive species and thereby reduced the corrosion rate in 0.1M NaCl. In addition, the comparison of the two activation energies (E_a^i) and (E_a), i.e., with and without inhibitor, respectively, provides an indication of the dependence of the protection of the film on the temperature. When $E_a^i > E_a$, the inhibitor adsorbs onto the substrate by electrostatic bonding **[20]**, which is sensitive to the temperature so that the corrosion resistance decreases by raising the temperature by desorption of the inhibitor.

The Nyquist and Bode plots of mild steel in 0.1M NaCl solution without and with the presence of 600 mg.L^{-1} of cerium nitrate inhibitor were recorded at the OCP after immersion samples for 30 minutes and at different temperatures are plotted in **Figs. 4a, b, c &b**. The results of EIS data are gathered in **Table 3**. Rs, Rc and Rct are the solution resistance, the resistance of the outer porous coating, and the charge transfer resistance at the interface; respectively. Thus, the constant phase elements CPEc and CPEdl are the non-ideal (dispersive) layer capacitance, and double-layer capacitance, respectively. Also, the n values represent a non-linear coefficient. The fitted results of the EIS data are illustrated in **Table 3**.

The EIS diagrams of mild steel (**Fig. 4a &b**) displayt two capacitive loops at intermediate and low frequencies (an equivalent circuit is proposed in the inset of **Figure 4a**). Thus, the size of Nyquist plots decreased with increasing the temperature, reflecting the decrease in transfer resistance (Rct). However, the value of Rc at low frequencies is clearly reduced with increasing the temperature, indicating the detachment of the corrosion products from the surface.

In the presence of inhibitor, all the EIS diagrams exhibited the same shape regardless of temperature. They show two uncoupled relaxation times at high-intermediate/low frequencies (an equivalent circuit is proposed in the inset of **Figure 4c**, for modeling the impedance data- **Table 3**-). However, it was observed that the size of Nyquist plots started to decrease with increasing the temperature of the solution. Indeed, **Table 3** shows that increasing the temperature leads to a decrease in Rct and an increase in CPE_{dl}values. This suggests that the films of corrosion products covering the mild steel surface have become porous and less adherent to the surface due to the physicochemical properties changes that allows the chloride ions and water to penetrate. Indeed, the increase of Rc with temperature suggests a gradual accumulation of a deposit on the surface that protects against corrosion.

The surface morphology monitoring experiments were conducted after polarization tests by using an optical microscope (MO), white light interferometer (WLI) and a scanning electronic microscope (SEM). from the MO images (**Fig. 5**) show that the samples without inhibitor undergo pitting corrosion which becomes more frequent with increasing bath temperature. This agrees with previous works showing that pitting corrosion initiates on pores of the corrosion product formed in halide-containing solutions **[21,22]**. However, in the presence of the corrosion inhibitor, the MO images presented in **Fig. 6** show the deposition of a thin protective layer but non-covering the entire surface of the substrate where the surface covering rate diminishes with increasing bath temperature.

To confirm the corrosion inhibition effect of the inhibitor, the surface morphology of the samples was also examined by WLI measurements and the results are presented in the 3D images shown in **Fig. 7**. The calculated parameters of the film are gathered in **Table 4**. It is clear from the WLI images that the average thickness of the film decreases with increasing bath

temperature (See also **Table 4**). It is noticed that the darker the color of the area or spots in the 3D images, plus the thickness of the deposit is low i.e. that the black areas are attributed to the surface of the substrate. The increase in average roughness values calculated by using FRT Mark III software (**Table 4**) can be attributed to the formation of a thin or a heterogeneous film on the surface of the substrate [23]. Moreover, it seems that the increase of the bath temperature decreases the grain size of the obtained deposits which may be due to the formation of a deposit rich in cerium oxide contrary to the deposits obtained at low bath temperature which rich in cerium hydroxide [3, 24].

The SEM images and the EDS spectra of the analysed specimens immersed in 0.1M NaCl + 600 mg.L^{-1} Ce(NO$_3$)$_3$ at different bath temperature are shown in **Fig. 8**. The amount of cerium (at %) in the film at different bath temperatures is given in **Table 5**.

The **Fig. 8a** shows the formation of inhomogeneous film that covered the entire surface of mild steel. The good stability of the film is due to the formation of both, cerium hydroxide and cerium oxide obtained by oxidation of the Ce^{3+}compounds [11]. The corresponding EDS spectrum of this figure (**Fig. 8a**) indicated that the film was rich in cerium (Ce) [11]. With the increase of the bath temperature, the film becomes more heterogeneous, contains cracks and with some surface defects (**Figs. 8b to 8d**). The cracks generated on the film can be due to the shear stresses between the film and the substrate [25]. Furthermore, the amount of Ce decreases with increasing bath temperature (**Table 5**). Consequently, the corrosion resistance of the film diminished and surface attack increased. These observations confirm again the results obtained with theelectrochemical techniques. Therefore, the films show poor thermal stability with increasing bath temperature.

4. Conclusion

From the results obtained in this work, it is concluded that:

- The presence of cerium nitrate inhibitor in corrosive solution containing a chloride ions increased the corrosion resistance of mild steel.

- The current density increased with increasing temperature of the bath in the absence and presence of cerium nitrate inhibitor in 0.1M NaCl solution.

- Increasing the temperature of the solution decreased the charge transfer resistance (Rct), and increased the CPE_{dl} and Rc with the presence of cerium nitrate inhibitors.

- The values of ΔH_a and ΔS_a suggest that the cerium inhibitor was mainly physisorbed to the surface of mild steel in 0.1M NaCl.

- The activation energies for the corrosion process to occur suggested that the inhibitor molecules adsorbed on the surface of the mild steel by electrostatic bonding, which is in agreement with the physisorption process revealed from the enthalpy values.

- The increase of the bath temperature allowed to decrease the average thickness and grain size of the film. Contrarily, the average roughness raised.

- The film seemed to be more heterogeneous and containing cracks with increasing the bath temperature.

References

[1] P. Bommersbach, C. Alemany-Dumont, J. P. Millet, B. Normand. Formation and behaviour study of an environment-friendly corrosion inhibitor by electrochemical methods, Electrochim. Acta. 51 (2005) 1076-1084.

[2] N. Um, T. Hirato. Precipitation of Cerium Sulfate Converted from Cerium Oxide in Sulfuric Acid Solutions and the Conversion Kinetics, Mater. Trans. 53 (2012) 1986-1991.

[3] Y. Hamlaoui, L. Tifouti, C. Remazeilles, F. Pedraza.Cathodic electrodeposition of cerium based oxides on carbon steel from concentrated cerium nitrate. Part II: Influence of electrodeposition parameters and of the addition of PEG, Mater. Chem. Phys. 120 (2010) 172-180.

[4] H. Y. Chang, H. I. Chen. Morphological evolution for CeO_2 nanoparticles synthesized by precipitation technique, J. Cryst. Growth. 283 (2005) 457-468.

[5] L. Arurault, P. Monsang, J. Salley, R. S. Bes. Electrochemical preparation of adherent ceria coatings on ferritic stainless steel, Thin Solid Films. 466 (2004) 75-80.

[6] Y. Zhou, J.A. Switzer. Growth of cerium(IV) oxide films by the electrochemical generation of base method, J. Alloy. Compd. 237 (1996) 1-5.

[7] K. Wang, Y. Chang, L. Lv, Y. LongSchool. Effect of annealing temperature on oxygen vacancy concentrations of nanocrystalline CeO_2 film, Appl. Surf. Sci. 351 (2015) 164-168.

[8] H. Boudellioua, Y. Hamlaoui, L. Tifouti, and F. Pedraza, Comparison between the inhibition efficiencies of two modification processes with PEG–ceria based layers against corrosion of mild steel in chloride and sulfate media.J. Mater. Eng. Perform. 26 (2017) 4402-4414.

[9] M. Hosseini, H. Ashassi-Sorkhabi, H. A. Yaghobkhani Ghiasvand. Corrosion protection of electro-galvanized steel by green conversion coatings, J. Rare. Earth. 25 (2007) 537-543.

[10] Y. Hamlaoui, H. Boudellioua, L. Tifouti, F. Pedraza. Corrosion resistance of electro-galvanized steel coated with PEG-modified ceria layers in chloride and sulfate media, J. Mater. Eng. Perform. 24 (2015) 4626-4635.

[11] H. Boudellioua, Y. Hamlaoui, L. Tifouti, and F. Pedraza, Effects of polyethylene glycol (PEG) on the corrosion inhibition of mild steel by cerium nitrate in chloride solution, Appl. Surf. Sci. 473 (2019) 449-460.

[12] Y. Hamlaoui, F. Pedraza, C. Remazeilles, S. Cohendoz, C. Rébéré, L. Tifouti, J. Creus.Cathodic electrodeposition of cerium-based oxides on carbon steel from concentrated cerium nitrate solutions. Part I: Electrochemical and analytical characterization, Mater. Chem. Phys. 113 (2009) 650-657.

[13] M.A. Arenas, A. Conde, J. J. de Damborenea.Cerium: a suitable green corrosion inhibitor for tinplate, Corros. Sci. 44 (2002) 511-520.

[14] K. Aramaki. Synergistic inhibition of zinc corrosion in 0.5M NaCl by combination of cerium (III) chloride and sodium silicate, Corros. Sci. 44 (2002) 871-886.

[15] M. Stern, A. L. Geary.Electrochemical Polarization I. A Theoretical Analysis of the Shape of Polarization Curves, J. Electrochem. Soc. 104 (1957) 56-63.

[16] E. Khamis. The Effect of Temperature on the Acidic Dissolution of Steel in the Presence of Inhibitors, Corrosion. 46 (1990) 476-484.

[17] M. Abdallah. Antibacterial drugs as corrosion inhibition for corrosion of Al in HCl solution, Corros. Sci. 46 (2004) 1981-1996.

[18] A. S. Fouda, A. A. Al-Sarawy, F. Sh-Ahmed, H. M. El-Abbasy. Corrosion inhibition of aluminium 6063 using some pharmaceutical compounds, Corros. Sci. 51 (2009) 485-492.

[19] S. Pournazari, M. H. Moayed, M. Rahimizadeh. In situ inhibitor synthesis from admixture of benzaldehyde and benzene-1,2-diamine long with $FeCl_3$ catalyst as a new corrosion inhibitor for mild steel in 0.5M sulphuric acid, Corros. Sci. 71 (2013) 20-31.

[20] A. Popova, E. Sokolova, S. Raicheva, M. Christov.AC and DC study of the temperature effect on mild steel corrosion in acid media in the presence of benzimidazole derivatives, Corros. Sci. 45 (2003) 33-58.

[21] E. Bardal, Corrosion and Protection; Springer-Verlag, London, UK (2004) p. 124.

[22] J. Tang, J. Li, H. Wang, Y. Wang and G. Chen.In-Situ monitoring and analysis of the pitting corrosion of carbon steel by acoustic emission, Appl. Sci. 9 (2019) 706-725.

[23] K. M. Shainy, P. R. Ammal, K. N. Unni, S. Benjamin, A. Joseph. Surface Interaction and Corrosion Inhibition of Mild Steel in Hydrochloric Acid Using Pyoverdine, an Eco-Friendly Bio-molecule, Journal of Bio- and Tribo-Corrosion 2(2016) 20.

[24] R. Sen, S. Das, K. Das. The effect of bath temperature on the crystallite size and microstructure of Ni–CeO2 nanocomposite coating, Mater. Charact. 62 (2011) 257-262.

[25] B. Bouchaud, J. Balmain, G. Bonnet, F. Pedraza, Optimizing structural and compositional properties of electrodeposited ceria coatings for enhanced oxidation resistance of a nickel-based superalloy, Appl. Surf. Sci. 268 (2013) 218–224.

Figure captions

Fig. 1. Potentiodynamic polarization curves for mild steel immersed for 30 min in 0.1M NaCl solution (a) without and (b) with cerium nitrate inhibitor, at different temperatures.
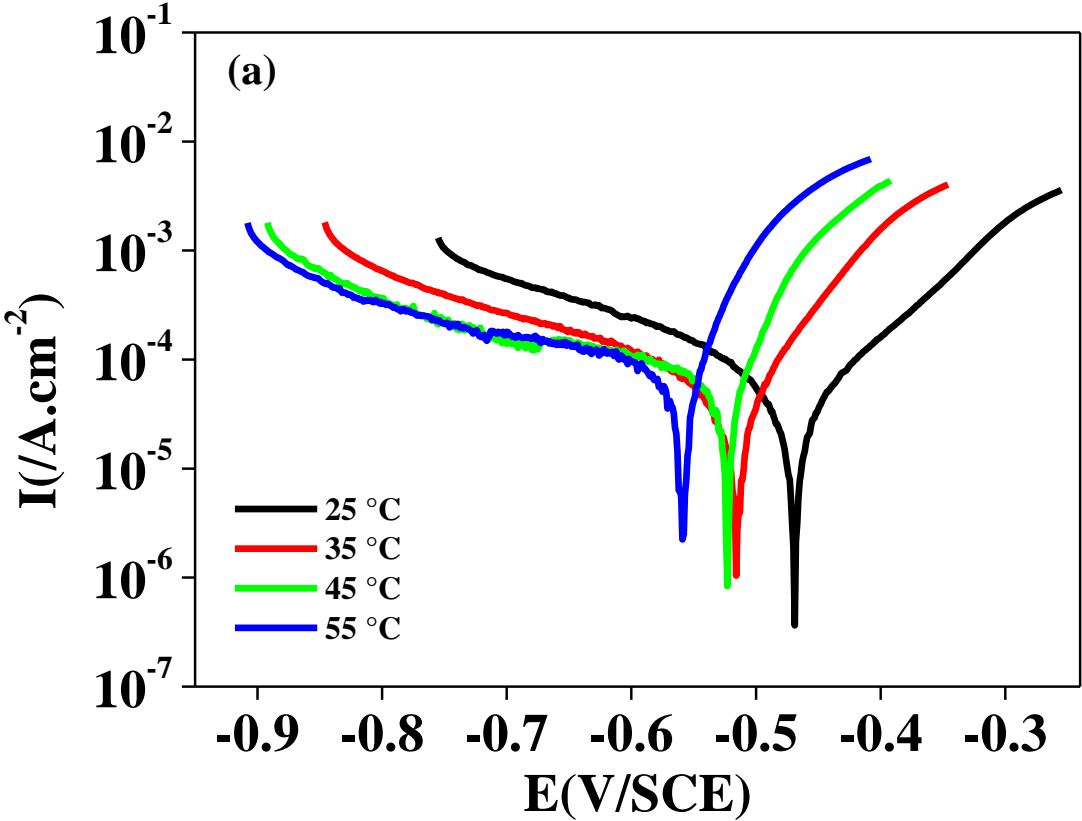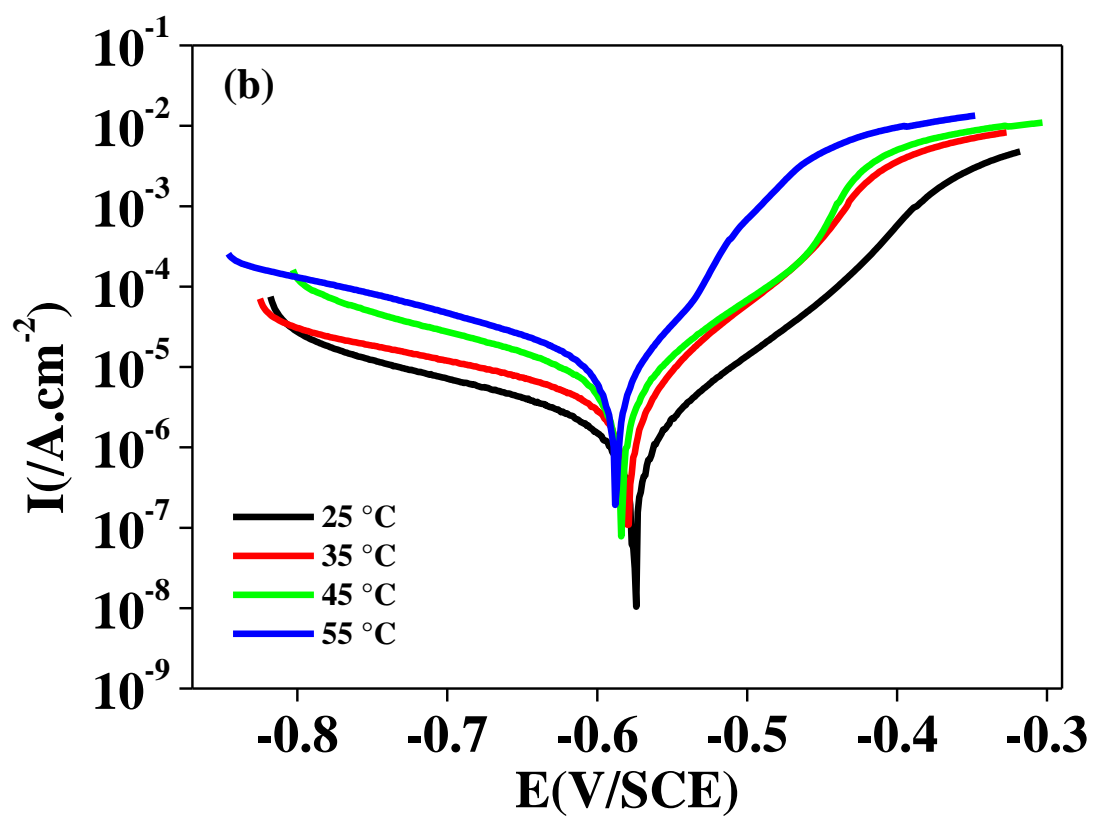
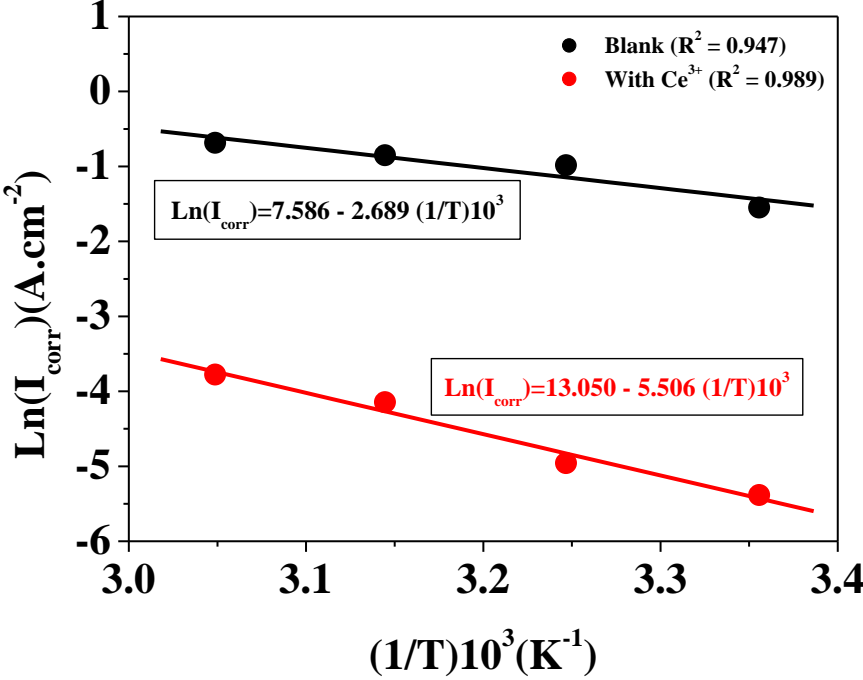**Fig. 2.** Arrhenius plots of mild steel immersed for 30 min in 0.1M NaCl solution with and without cerium nitrate inhibitor.

Fig. 3. Arrhenius plot of mild steel $Ln(I_{corr}/T)$ versus $(1/T)$ immersed for 30 min in 0.1M NaCl solution with cerium nitrate inhibitor.
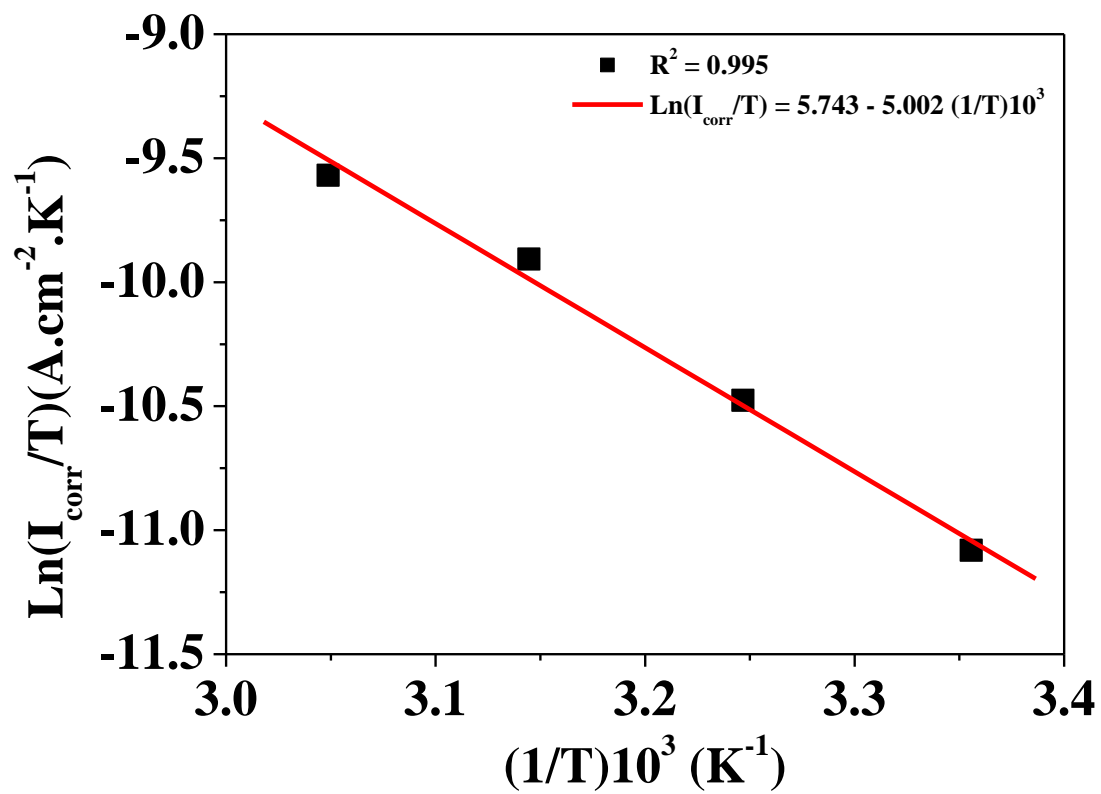
Fig. 4. EIS diagrams (a & c) Nyquist and (b & d) Bode plots for mild steel after 30 min of immersion in 0.1M NaCl solution without (bare) and with 600 mg.L^{-1} of cerium nitrate, respectively ; at different temperatures.
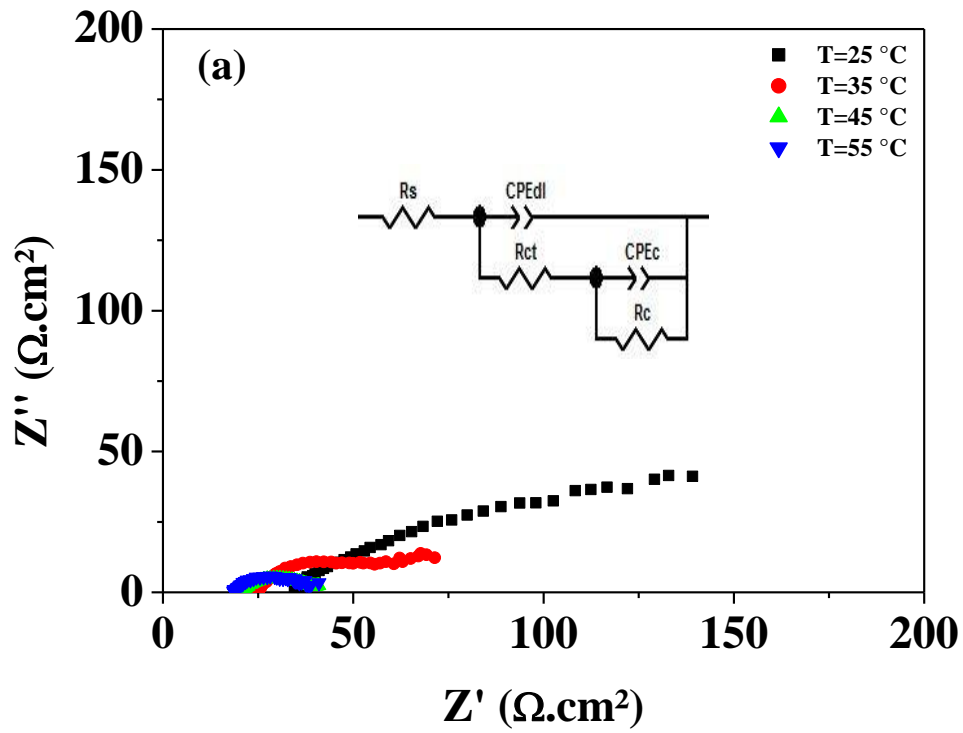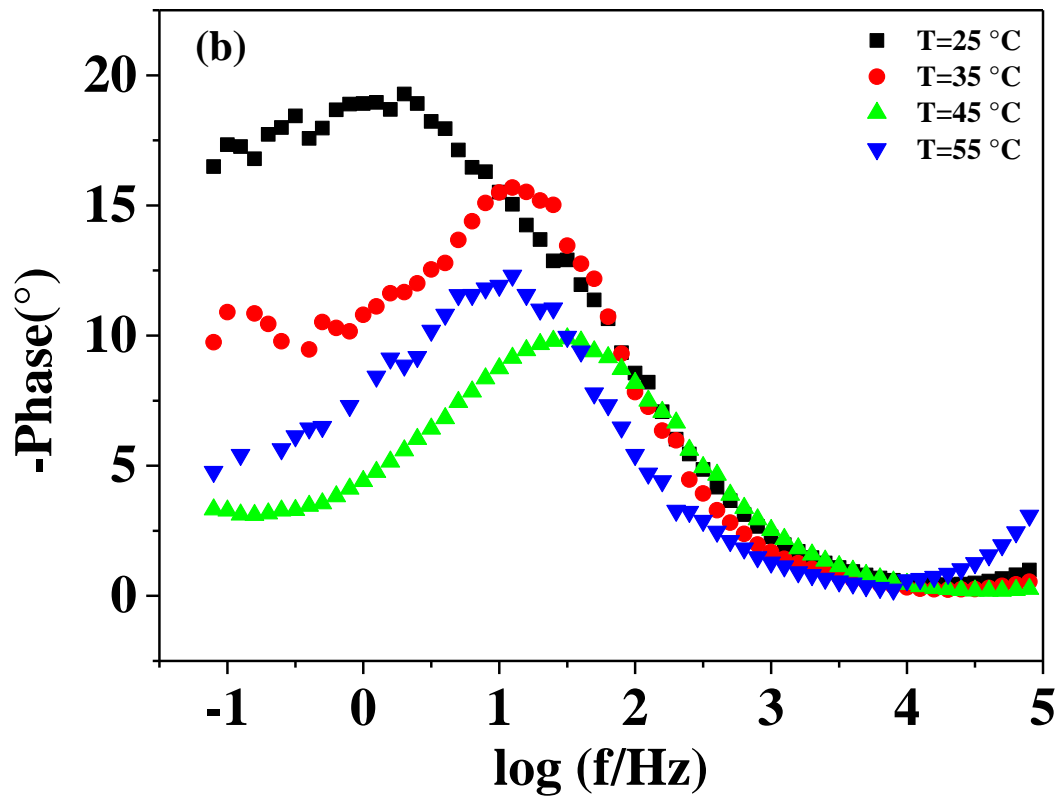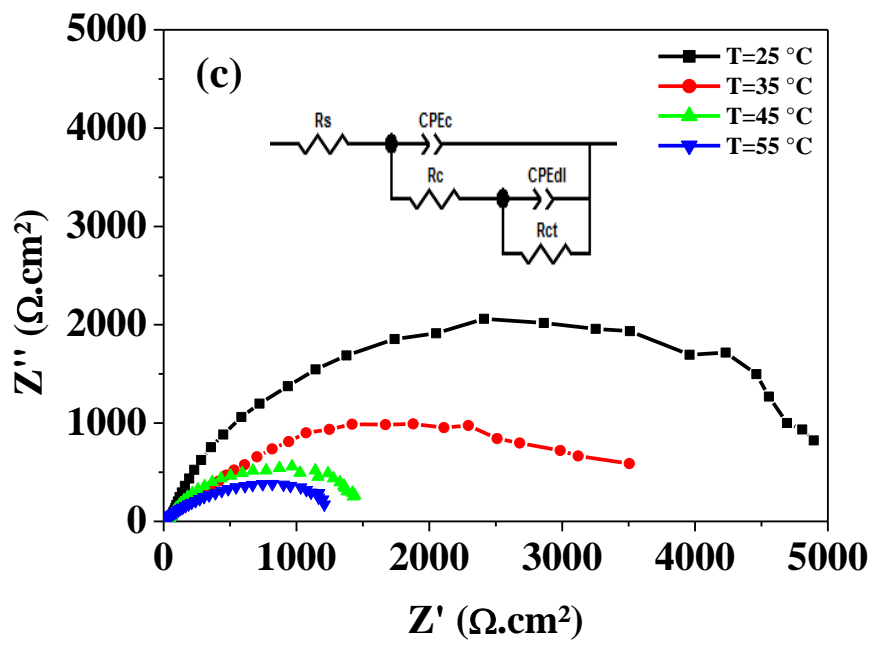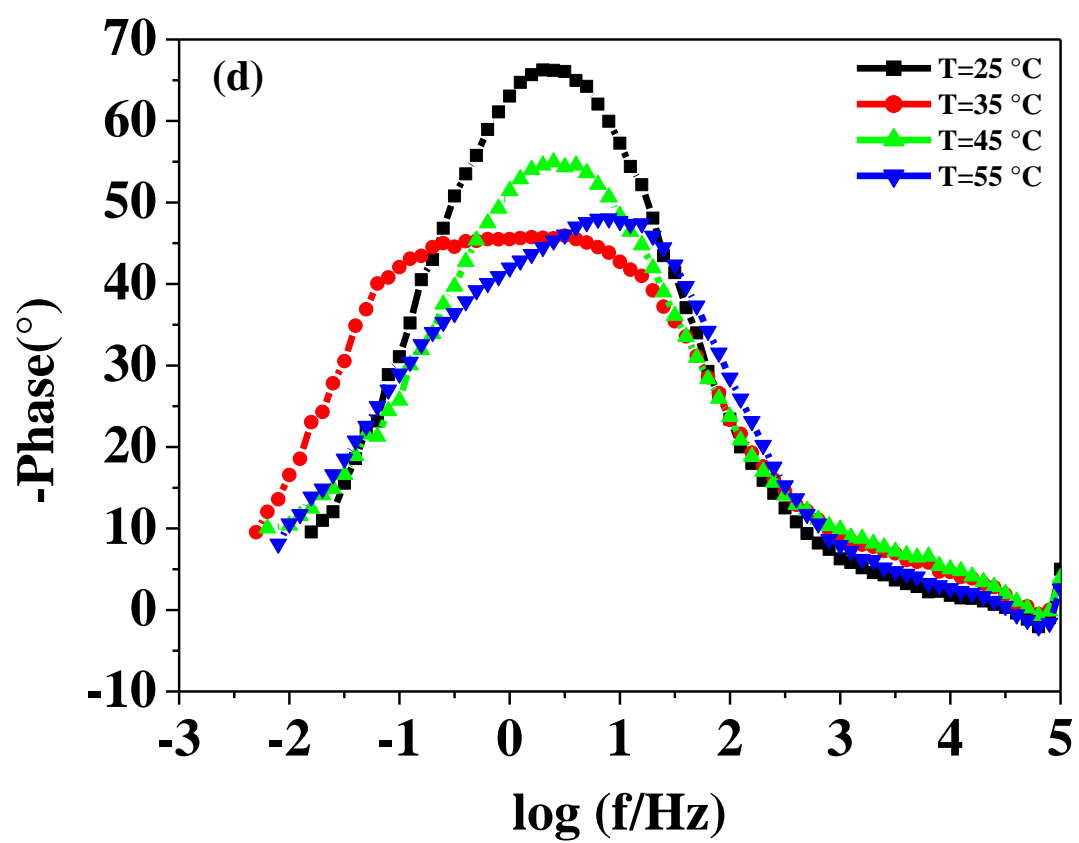
Fig. 5. Corrosion attack surface morphologies for the substrate after polarization test in 0.1M NaCl without inhibitor addition at bath temperature (a) 25 (b) 35 (c) 45 and (d) 55 °C.

Fig. 6. Corrosion attack surface morphologies for the substrate after polarization test in 0.1M NaCl with the presence of 600 mg.L^{-1} of cerium nitrate at bath temperature (a) 25 (b) 35 (c) 45 and (d) 55 °C.

Fig. 7. WLI (3D) images of the surface morphologies for the substrate after polarization test in 0.1M NaCl with the presence of 600 mg.L^{-1} of cerium nitrate at bath temperature (a) 25 (b) 35 (c) 45 and (d) 55 °C.

Fig. 8. SEM surface morphologies of substrate after polarization test in 0.1M NaCl with the presence of 600 mg.L^{-1} of cerium nitrate at bath temperature (a) 25 (b) 35 (c) 45 and (d) 55 °C and the corresponding EDS spectra

Fig. 1. Potentiodynamic polarization curves for mild steel immersed for 30 min in 0.1M NaCl solution (a) without and (b) with cerium nitrate inhibitor, at different temperatures.

Fig. 1a.

Fig. 1b.

Fig. 2. Arrhenius plots of mild steel immersed for 30 min in 0.1M NaCl solution with and without cerium nitrate inhibitor.

Fig. 3. Arrhenius plot of mild steel Ln(I_{corr}/T) versus (1/T) immersed for 30 min in 0.1M NaCl solution with cerium nitrate inhibitor.

Fig. 4. EIS diagrams (a & c) Nyquist and (b & d) Bode plots for mild steel after 30 min of immersion in 0.1M NaCl solution without (bare) and with 600 mg.L^{-1} of cerium nitrate, respectively ; at different temperatures.

Fig. 4a.

Fig. 4b.

Fig. 4c.

Fig. 4d.

Fig. 5. Corrosion attack surface morphologies for the substrate after polarization test in 0.1M NaCl without inhibitor addition at bath temperature (a) 25 (b) 35 (c) 45 and (d) 55 °C.
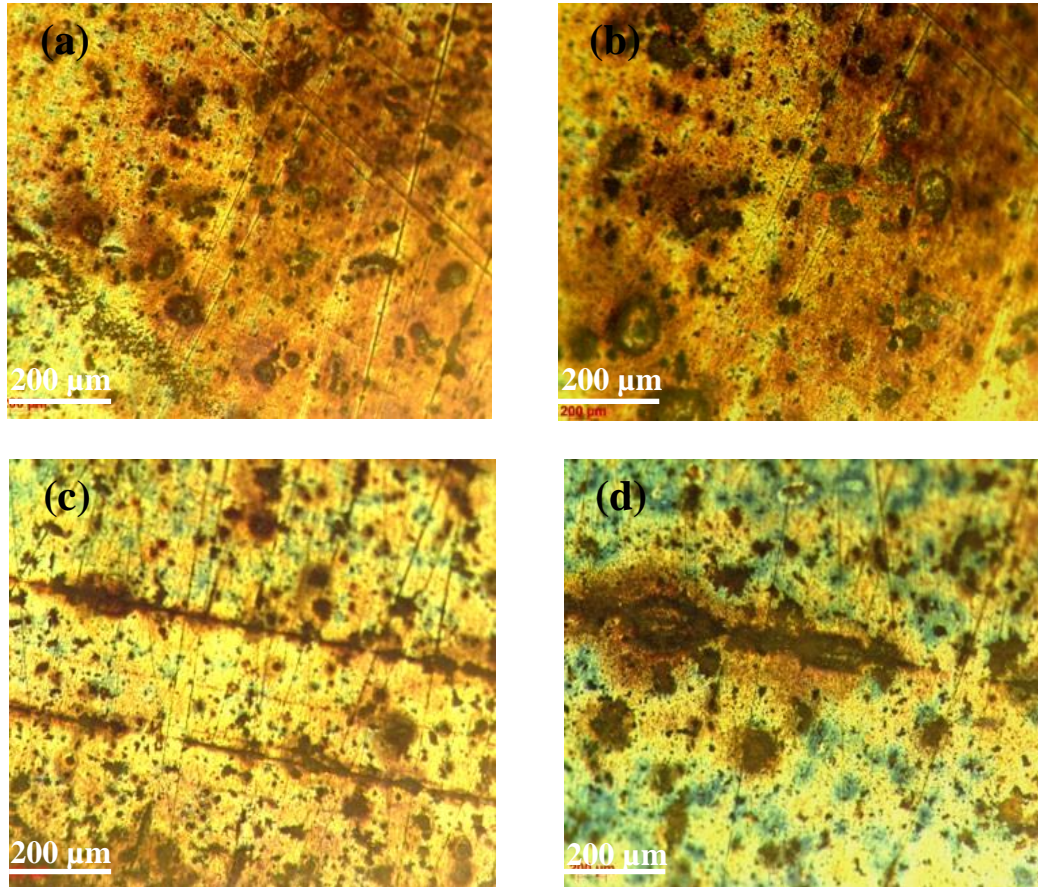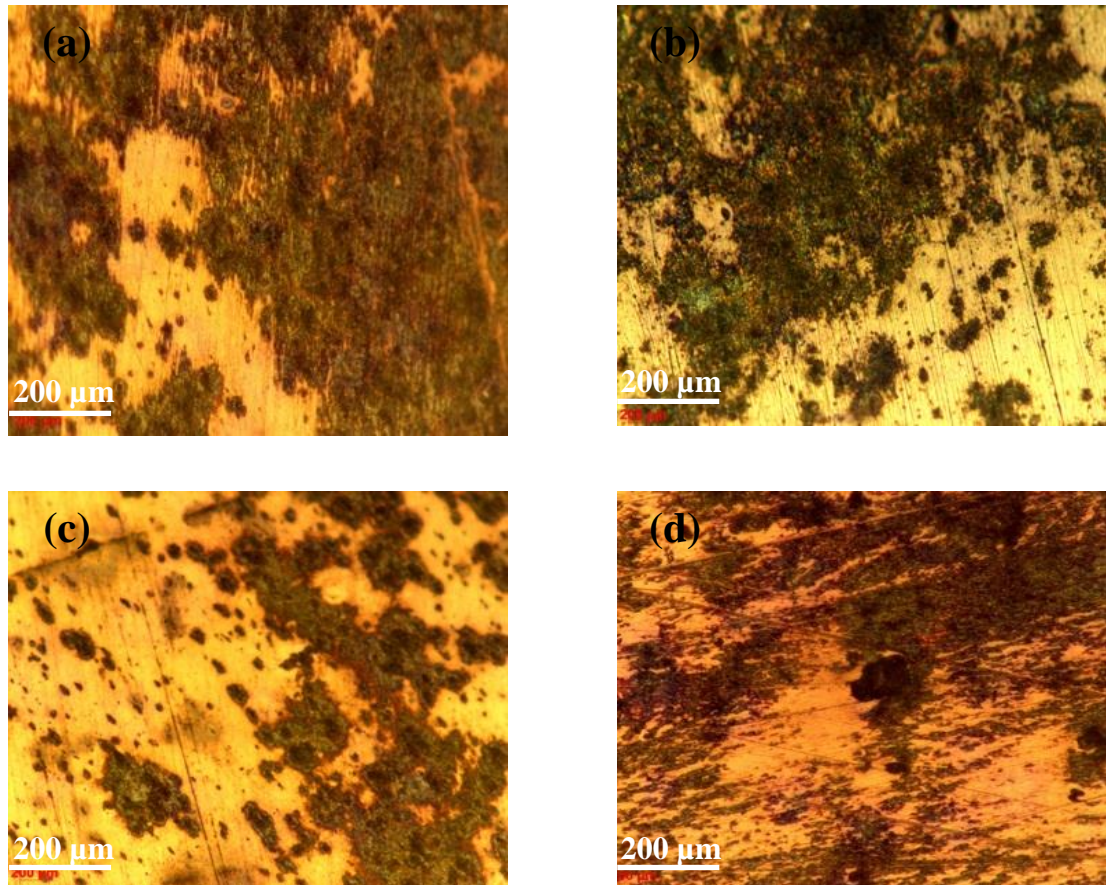

Fig. 5a, b, c & d.

Fig. 6. Corrosion attack surface morphologies for the substrate after polarization test in 0.1M NaCl with the presence of 600 mg.L^{-1} of cerium nitrate at bath temperature (a) 25 (b) 35 (c) 45 and (d) 55 °C.
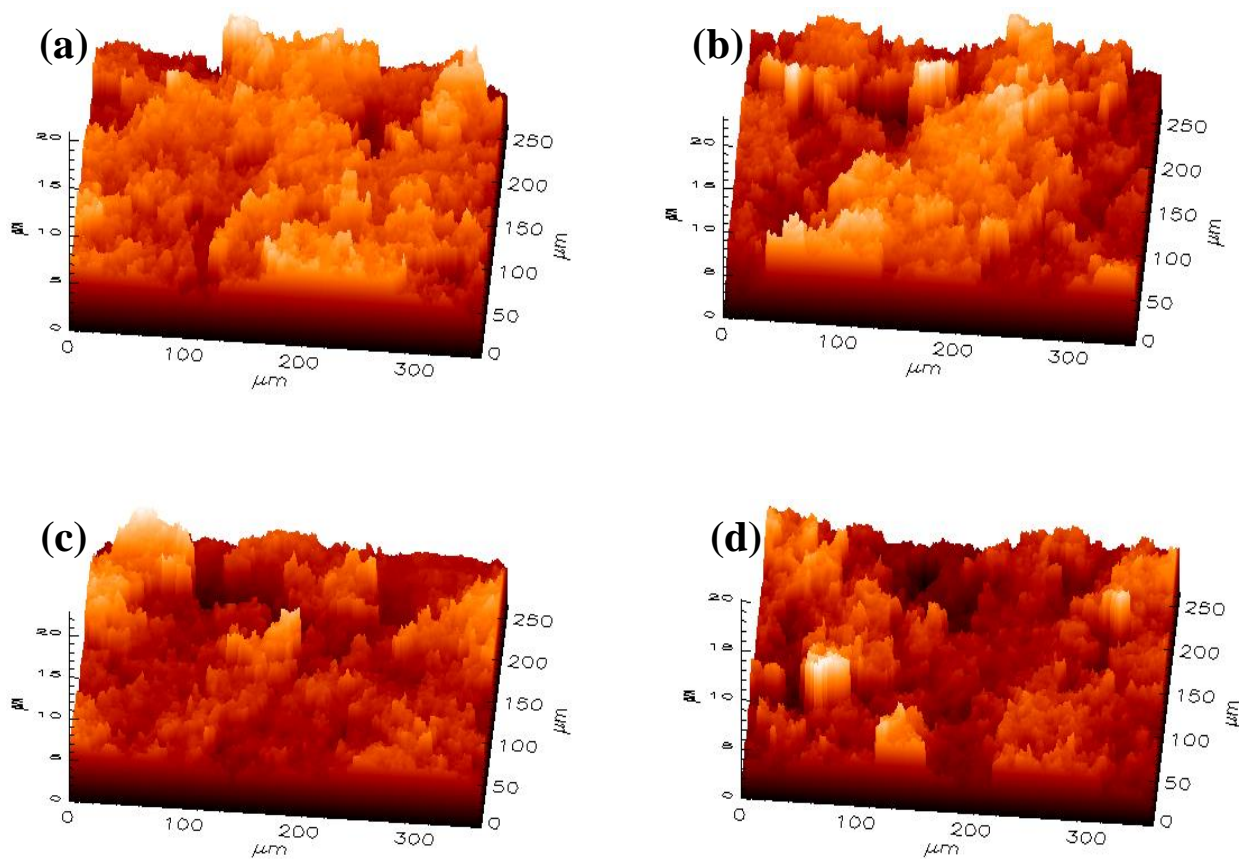

Fig. 6a, b, c & d.

Fig. 7. WLI (3D) images of the surface morphologies for the substrate after polarization test in 0.1M NaCl with the presence of 600 mg.L^{-1} of cerium nitrate at bath temperature (a) 25 (b) 35 (c) 45 and (d) 55 °C.
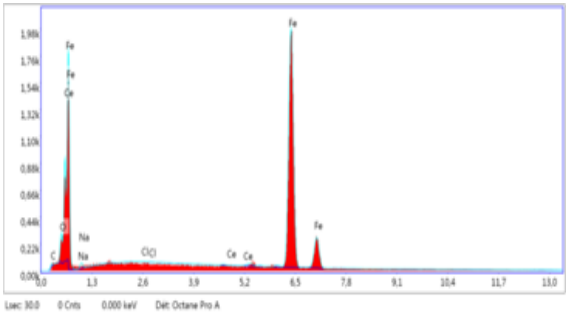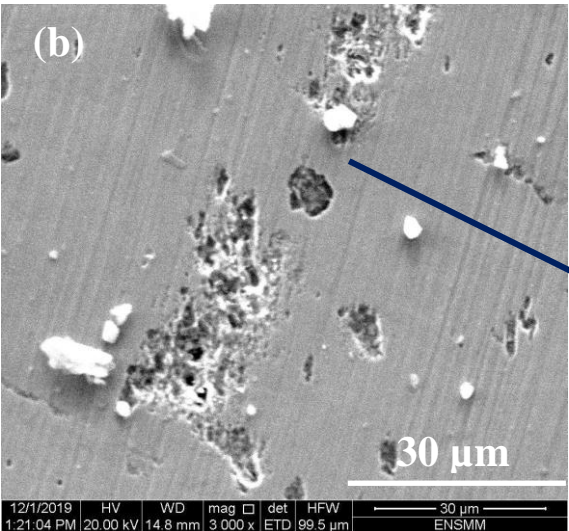

Fig. 7a, b, c & d.

Fig. 8. SEM surface morphologies of substrate after polarization test in 0.1M NaCl with the presence of 600 mg.L-1 of cerium nitrate at bath temperature (a) 25 (b) 35 (c) 45 and (d) 55 °C and. With the corresponding EDS spectrum.
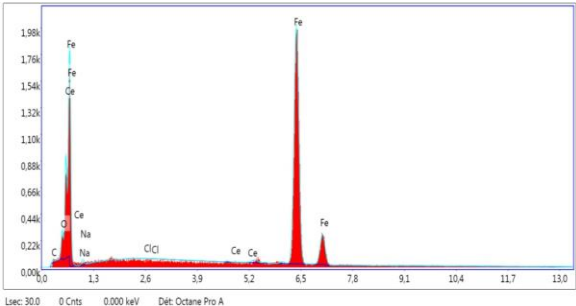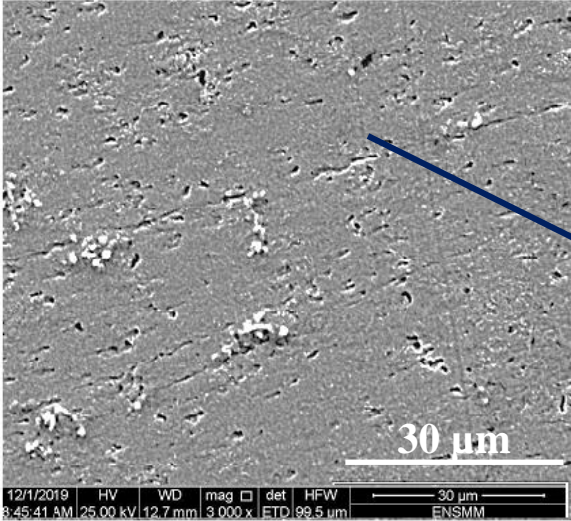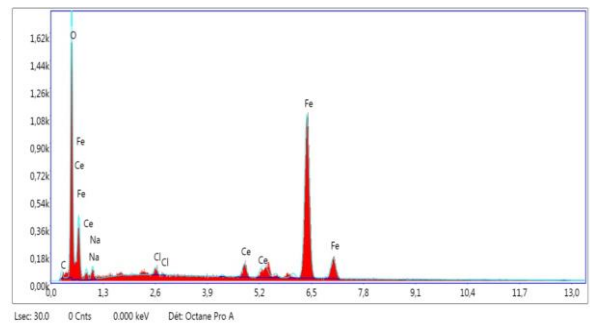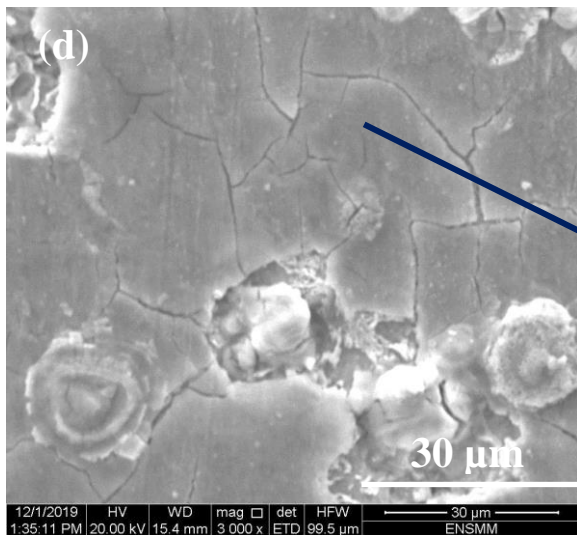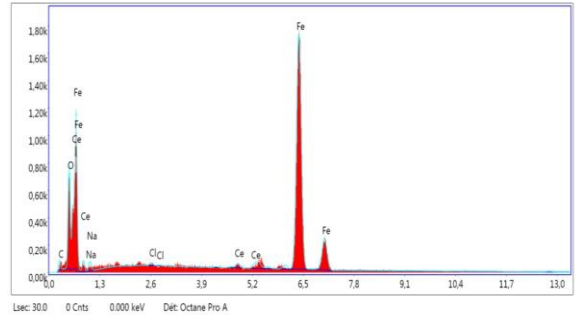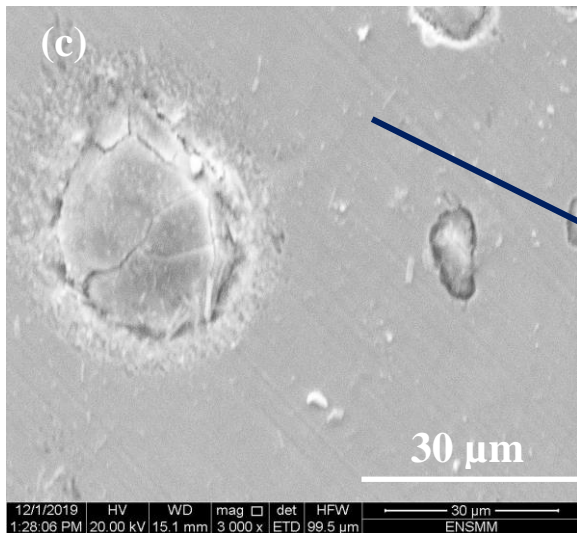
Fig. 8a, b, c & d.

Table captions

Table 1. Polarization parameters and the corresponding surface coverage for mild steel in 0.1M NaCl in the absence (bare) and in the presence of 600 mg.L^{-1}of cerium nitrate at different temperatures.

Sample	Temperature (°C)	E$_{corr}$ (mV/SCE)	βa (mV/dec)	I$_{corr}$ (μA/cm²)	θ	Rp (Ω cm²)
Bare mild steel	25	-486	111.0	148.9	----	227
	35	-515	90.2	319.7	----	105
	45	-523	80.5	387.1	----	82
	55	-558	83.6	472.8	----	72
With Ce^{3+}	25	-574	62.5	4.59	0.97	5919
	35	-579	61.6	7.03	0.97	3806
	45	-583	59.2	15.84	0.96	1625
	55	-587	64.8	22.91	0.95	1224

Table 2. Corrosion kinetics and thermodynamic parameters for mild steel immersed for 30 min in 0.1M NaCl with and without the presence of cerium nitrate inhibitor.

	Thermodynamic parameters		
	E$_a$ (kJ/mol)	ΔHa (kJ/mol)	ΔSa (j/mol.K)
0.1 M NaCl	22.34	----	----
with Ce^{3+}	45.75	-41.58	- 24.54

Table 3. Fitting results for the EIS data for mild steel electrode without (bare) and with the presence of cerium nitrate inhibitor in 0.1M NaCl at different temperatures.

Sample	Temperature (°C)	Rs (Ω cm^2)	n_c	CPE$_c$ (F cm^{-2} s$^{(1-n)}$)	Rc (Ω.cm^2)	n_{dl}	CPE$_{dl}$ (F cm^{-2} s$^{(1-n)}$)	Rct (Ω cm^2)
Bare mild steel	25	34.04	0.5	0.011019	149.7	0.56	0.002734	78.12
	35	24.90	0.5	0.034171	62.81	0.77	0.001196	27.18
	45	20.71	0.48	0.139950	8.11	0.70	0.001687	16.45
	55	18.75	0.5	0.087252	10.88	0.74	0.002864	14.68
with Ce^{3+}	25	40.30	0.81	12.9 10^{-5}	34	0.88	8.1 10^{-5}	5229
	35	25.60	0.78	7 10^{-5}	70	0.61	6.0 10^{-5}	3830
	45	22.49	0.70	5 10^{-5}	85	0.89	1.9 10^{-5}	1660
	55	15.45	0.62	3 10^{-5}	120	0.75	1.1 10^{-5}	1280

Table 4. Surface parameters of the substrate after polarization tests realized in 0.1M NaCl with the presence of 600 mg.L^{-1} of cerium nitrate at different bath temperature.

Bath temperature (°C)	Thickness (μm)	Grain size (μm)	Roughness (μm)
25	2.99	0.230	0.445
35	2.78	0.143	0.449
45	1.89	0.111	0.492
55	0.85	0.015	0.506

Table 5. The percentageof the cerium (at %) in the film correspnding with EDS spectrum of the substrate after polarization tests realized in 0.1M NaCl with the presence of 600 mg.L^{-1} of cerium nitrate at different bath temperature.

	Bath temperature (°C)			
	25	**35**	**45**	**55**
Ce (at %)	9.40	8.39	5.52	1.19